Coherent magnetotransport in confined arrays of antidots. III. Origin of the commensurate peaks

I. V. Zozoulenko
Department of Physics and Measurement Technology, Linköping University, S-581 83 Linköping, Sweden

Frank A. Maaø and E. H. Hauge
Department of Physics, Norwegian University of Science and Technology, N-7034, Trondheim, Norway
(Received 14 March 1997; revised manuscript received 24 April 1997)

We study coherent magnetotransport in finite antidot arrays in four-terminal geometry. The calculated longitudinal resistance is in very good agreement with experimental data. The quantum-mechanical current density is visualized, and we discuss its relation to classical electron dynamics. A pronounced commensurate peak in the longitudinal resistance is attributed to the enhancement of the transmission in the transverse direction due to runaway trajectories. [S0163-1829(97)01131-4]

I. INTRODUCTION

A periodic potential applied to a high-mobility two-dimensional electron gas defines arrays of islands, called antidots, which are nontransparent for electrons. Experimental studies of magnetotransport in antidot arrays revealed a series of pronounced broad peaks in the diagonal magnetoresistivity ρ_{xx}, which are believed to occur when commensurability conditions are fulfilled between the superlattice period and the classical cyclotron radius $r_c=\hbar k_F/eB$ at the Fermi momentum $\hbar k_F$.[1–6] See Refs. 7,8 for an extensive list of further references. The semiclassical explanation of the magnetoresistance maxima is that electrons are pinned in orbits around (or between) groups of antidots for a long time and, therefore, do not contribute to the conductivity.[9] Since the experimental data seemed to be explained by it, the above picture was widely accepted as correct.

However, an alternative explanation of the experimental data was put forward by Baskin *et al.*[10] who found that stable ''runaway'' trajectories, rolling along different rows of the antidot lattice, are responsible for an enhancement of the diagonal *conductivity* σ_{xx}. Runaway trajectories were recently used by Schuster *et al.*[11] in the interpretation of their experiments. They found that the off-diagonal terms of the resistivity tensor play an important role and that pronounced maxima in the magnetoresistance correspond not to minima in the conductance as one could expect, but to *maxima*, consistent with the existence of runaway trajectories. Similar conclusions outlining the importance of the runaway trajectories have recently been reported by Tsukagoshi *et al.*[12] and Kaiser *et al.*[13]

Quantum-mechanical calculations of the magnetoconductance of antidot lattices have been performed by a number of groups,[16–20] and good agreement between numerical results and observed features in the magnetoresistance has been found. However, in contrast to the semiclassical simulations, it is not always possible to directly relate these results to particular types of semiclassical trajectories dominating the electron dynamics.

In addition to the gross features in the the magnetoconductivity, a fine structure superimposed on the commensurability peaks has been detected in subsequent experiments.[5,14,15] These features were successfully explained, both within the framework of the semiclassical periodic orbit theory,[14,18,19,21] and quantum mechanically.[16–20]

So far, the majority of experimental and theoretical work has concentrated on essentially *macroscopic* structures made up of thousands of antidots, such that the sample size well exceeds the length scale of inelastic scattering. Recently, magnetotransport in a *mesoscopic* sample with total dimensions smaller than the phase coherence length was studied.[22] Again, like in macroscopic samples, the diagonal resistance exhibits pronounced features when the cyclotron orbits fit around a certain number of antidots. In addition, phase coherence effects manifest themselves in reproducible quantum fluctuations superimposed onto the commensurate peaks.

In the preceding papers,[7,8] hereafter called I and II, we discussed coherent magnetotransport in mesoscopic arrays of antidots in confined geometry. In paper I we calculated magnetoband structure of infinite arrays, and visualized the current density of a number of Bloch states for different magnetic fields. In particular, at magnetic fields close to $B=B_c$, when, by definition of B_c, the cyclotron diameter equals the lattice constant of the array, the magnetobands correspond mostly to states of the runaway type, in which electrons bounce off antidots in consecutive unit cells. On the basis of the results obtained, the two-terminal conductance of finite arrays was analyzed in paper II. Unfortunately, the calculated two-terminal conductance could not be directly related to the experimental data. The experiments were done on samples with four-terminal geometry, in which the longitudinal and Hall resistances, R_L and R_H, were measured. Thus, the connection between theory and experiment remained somewhat conjectural. Besides, the calculated conductance was analyzed on the basis of the spatial features of Bloch states. It is not *a priori* evident that these features would survive in a finite lattice connected to leads. They could easily be obscured by mixing between different Bloch states and/or incoming and reflected electron flows.

The purpose of the present work is to study the four-terminal transport characteristics of finite antidot arrays. We

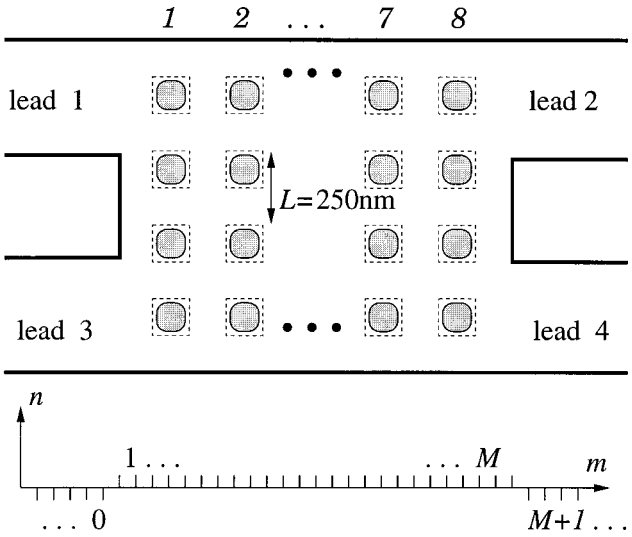

FIG. 1. Schematic geometry of the periodic antidot lattice in four-terminal geometry. Hard wall confinement is assumed. Antidots are modeled by a square potential with the height just above the Fermi energy, $V=1.05E_F$ (dashed squares). Due to the finite tunneling probability this potential corresponds to ''soft'' antidots with effectively rounded corners, as illustrated in the figure.

calculate the longitudinal and the Hall resistances of such a device, and find very good agreement with experimental data.[22] We visualize the current density in the corresponding two-terminal array, and find that it is closely related to the character of Bloch states in the infinite lattice. Analysis of the detailed spatial character of the current density reveals its relationship to the semiclassical dynamics. This is the strength of the present quantum approach as compared to those based directly on the Kubo formula: We can, like the classical simulations, reveal the dynamics underlying the conductance results. In particular, we find that the transmission probabilities between certain leads are strongly enhanced around the magnetic field of the commensurate ''resonance,'' $B=B_c$. The corresponding four-terminal longitudinal resistance (computed on the basis of the calculated transmission probabilities, within the framework of the Landauer-Büttiker formalism[23,24]) shows a pronounced maximum, in agreement with experimental findings.[22] At the same time, the current density exhibits striking features resembling the classical runaway trajectories. This allows us to rule out the hypothesis of pinned orbits and, instead, pinpoint the runaway mechanism as the one behind the commensurate peaks in a finite antidot lattice.

II. RESULTS AND DISCUSSION

The geometry of the structure under investigation is illustrated in Fig. 1. The parameters of the antidot lattice are the same as those used in papers I, II. They are chosen to closely match the experimental arrays studied by Schuster *et al.*[22] We consider an 8×4 square lattice of antidots with lattice constant $L=250$ nm. The antidots are modeled by a square potential with a height just above the Fermi energy, $V=1.05E_F$. Because of the finite tunneling probability through the corners, this potential corresponds to effectively rounded antidots with ''soft'' edges. Therefore, in the subsequent figures illustrating the current density pattern (see below), the antidots are shown with their effective shape, rather than as nominal squares. Further justification for this choice of antidot potential is given in paper I. The geometrical size of the antidots, $L/2$, equals the distance between them. However, taking into account the finite tunneling probability, an effective antidot size is somehow smaller than $L/2$. Four ideal leads of width $w=400$ nm are attached to the corners of the system. The calculated transport characteristics do not depend critically on the width of the leads, provided that they are sufficiently wide (i.e., they can support at least 5–10 propagating modes). All calculations have been performed in a one-particle picture with effective potentials, and with spin degeneracy assumed.

Experimentally, four-terminal resistances $R_{ij,kl}=(V_k-V_l)/I$ are obtained by passing a current I through the contacts i and j and measuring the voltage drop across the other two contacts (k and l). We calculate the longitudinal, $R_L=R_{12,34}$ and and the Hall resistance, $R_H=R_{14,32}$, on the basis of the Landauer-Büttiker formalism,[23,24] which relates the resistance of a structure to its scattering characteristics. This requires the calculations of all total transmission and reflection coefficients T_{ji}, R_{ii}, from lead i to lead j (the numbering of the leads is indicated in Fig. 1). We compute transmission coefficients on the basis of the hybrid Green function technique introduced in papers I and II, generalized here for the presence of four leads and finite temperature. Although the experiments have been performed at a base temperature of $T\approx0.03$ K, we use $T=1$ K in our calculations. This enhanced temperature takes Joule heating and randomness due to electron-electron interactions into account, in naive fashion.

Figure 2(a) shows the transmission coefficients for electrons entering the antidot array via the left lead 1. The mirror symmetry of our device, implies that transmission from a lead on the right is identical to that of the corresponding one on the left, and $T_{23}=T_{41}$, $T_{21}=T_{34}$, etc. Furthermore, time reflection invariance with $B\rightarrow-B$ gives, $T_{14}=T_{41}=T_{23}=T_{32}$. If the device would have fourfold rotational symmetry, all leads would be equivalent. Our calculations show that, although the symmetry is broken in our device, the symmetry breaking is sufficently small that T_{13} is qualitatively similar to T_{21}, and T_{43} to T_{31}. Consequently, we only show the coefficients for transmission out of lead 1.

Figures 2(b) and 2(c) show the calculated R_H, R_L, and two-terminal resistance, R_{2t}. The latter is computed in the two-terminal geometry when the leads 3 and 4 are disconnected. We note the following relation between the three, $R_{2t}\approx R_L+R_H$.[25] This reflects the fact that the Hall resistance represents a contribution mainly from the edge states, whereas the longitudinal resistance corresponds mainly to states propagating in the bulk (i.e., inner region). On the other hand, the two-terminal resistance includes contributions from all states.

The calculated longitudinal resistance, R_L, is in very good agreement with the corresponding curve of the experiment of Schuster *et al.* (Fig. 2 in Ref. 22). The calculated dependence not only reproduces the positions of the two broad maxima at $B\sim0.2$ T and $B\sim$ 0.7 T but also their relative height. The Fourier transform of the magnetoresistance oscillations, performed in a window of magnetic fields

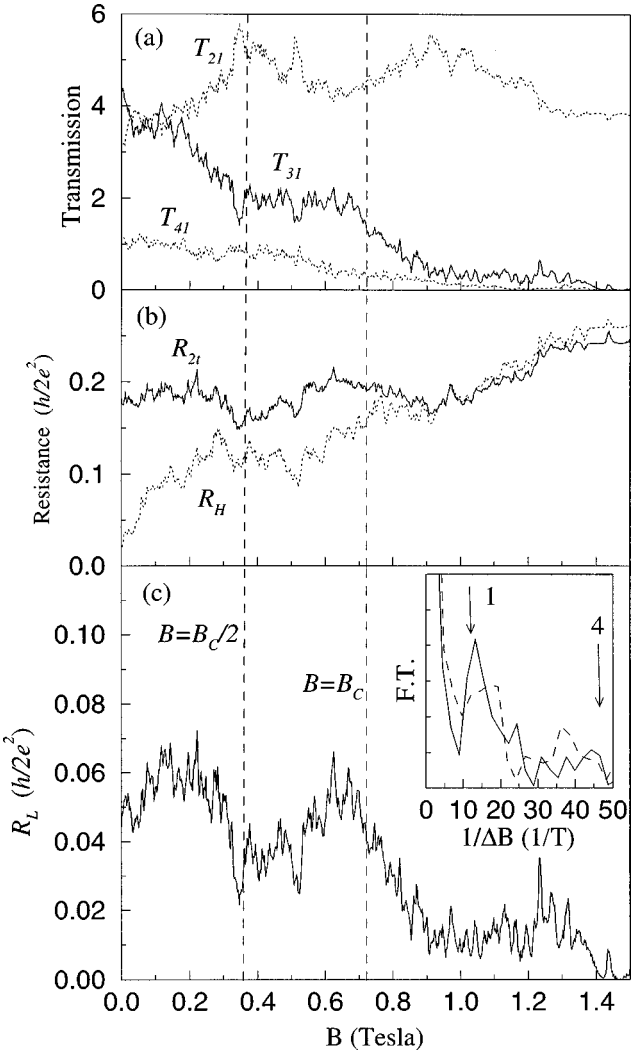

FIG. 2. (a) The transmission coefficients for electrons entering the antidot array via lead 1. (b) The two-terminal magnetoresistance R_{2t} and the four-terminal Hall resistance, R_H. (c) The longitudinal R_L resistance. The inset in (c) shows the Fourier Transform of R_L performed in the window ($0.4\ \mathrm{T}<B<0.8\ \mathrm{T}$) of the magnetic field near B_c (solid lines); and in the window $0<B<0.4$ T (dashed lines). Arrows indicate the magnetic fields of Aharonov-Bohm periodicity associated with cyclotron orbits around one and four antidots. The temperature is chosen as $T=1$ K, and the sheet electron density is $n_s=3\times10^{15}m^{-2}$. Finally, $B_c=\hbar k_F/eL$ is the magnetic field when the cyclotron diameter equals the lattice constant, L, of the array.

around B_c, reveals a pronounced peak corresponding to the periodicity $1/\Delta B=12\ \mathrm{T}^{-1}\approx L^2e/h$, where L^2 is the area of one lattice cell (see inset in Fig. 2, and note that the window chosen fixes the resolution of the corresponding Fourier spectrum). At lower magnetic fields, $B<0.4$ T, a second peak appears, $1/\Delta B\approx40\mathrm{T}^{-1}$, which approximately corresponds to the area of four unit cells. These findings are also consistent with the experimental observation of Ref. 22. A detailed discussion of the periodicity of the conductance oscillations and their relation to the oscillating part of the number of states in the antidot lattice, and to the Aharonov-Bohm effect, is given in paper II.

Before we proceed to a discussion of the calculated magnetoconductance, it is useful to visualize the quantum-mechanical current density, $\mathbf{j}(x,y)$, in our finite lattice, and compare it with the character of the Bloch states in the corresponding infinite lattice (studied in paper I). In principle, we should have calculated the current densities for the same four-terminal geometry as that used to compute R_L and R_H. However, a major reduction in computational effort was achieved by using the two-terminal geometry instead. Note that at relatively high magnetic field the Lorentz force confines incoming electron flow to the boundaries of the structure. This makes the two-terminal geometry effectively equal to a four-terminal one [see Figs. 3(d)–3(e)]. At low magnetic fields we intentionally confine the electron flow to the upper boundary by choosing an appropiate linear combination of the basic states. The physical picture emerging from these finite lattice calculations can be directly used in the interpretation of our four-terminal conductances.

Figure 3 shows current density patterns $\mathbf{j}(x,y)$ for several representative values of the magnetic field chosen on the interval $0<B<2B_c$. The direction of the magnetic field chosen here corresponds to counterclockwise cyclotron motion. At zero magnetic field the current predominantly flows between rows of antidots in the longitudinal direction. This is consistent with the character of the Bloch states in the infinite arrays. The latter consists of fast states with essentially one-dimensional laminar type flow channeling between rows of antidots, and slower ones with a genuinely two-dimensional flow of vortex character. Combination of the two results in some admixture of vortices, as seen in Fig. 3(a). Note that the classical simulations[15,26] reveal a similar character of electron dynamics at zero field. With increase of the magnetic field, the predominantly one-dimensional character of the current density gradually transforms into a complex flow of vortex type [Fig. 3(b)], reflecting a corresponding transformation of the Bloch states. However, in the field region near $B=0.35$ T (which roughly corresponds to the classical cyclotron motion around four antidots, $B\approx B_c/2$), the laminar quasi-one-dimensional flow along rows of antidots is again dominant, Fig. 3(c). Note that this is accompanied by an increase of the corresponding transmission probability, T_{21}.

Figure 3(d) shows a current density pattern calculated in the vicinity of the magnetic field $B=B_c$. The formation of edge states in which electrons skip along the upper boundary of the structure is clearly seen. At this value of the magnetic field, most of the bulk states in the infinite array are of the runaway type. This can be clearly traced in the current density pattern in the finite lattice. In particular, a significant part of the electrons in the bulk (i.e., those which do not skip along the upper edge of the system) run away along the leftmost column of antidots from lead 1 to lead 3. It is worth mentioning that the corresponding transmission coefficient, T_{31}, is enhanced, relatively speaking, in this field region. When the magnetic field is increased beyond the classical commensurability ''resonance'' at B_c, transport in the infinite lattice is mediated by states (beyond the edge states) which are localized around antidots or in the space between antidots. This is clearly manifested in the current density of the finite array, as shown in Fig. 3(e). Finally, at high magnetic field $B\gtrsim2B_c$, the incoming electron flow is spatially squeezed by the Lorentz force to an interval smaller than the distance between the upper row of antidots and the edge of

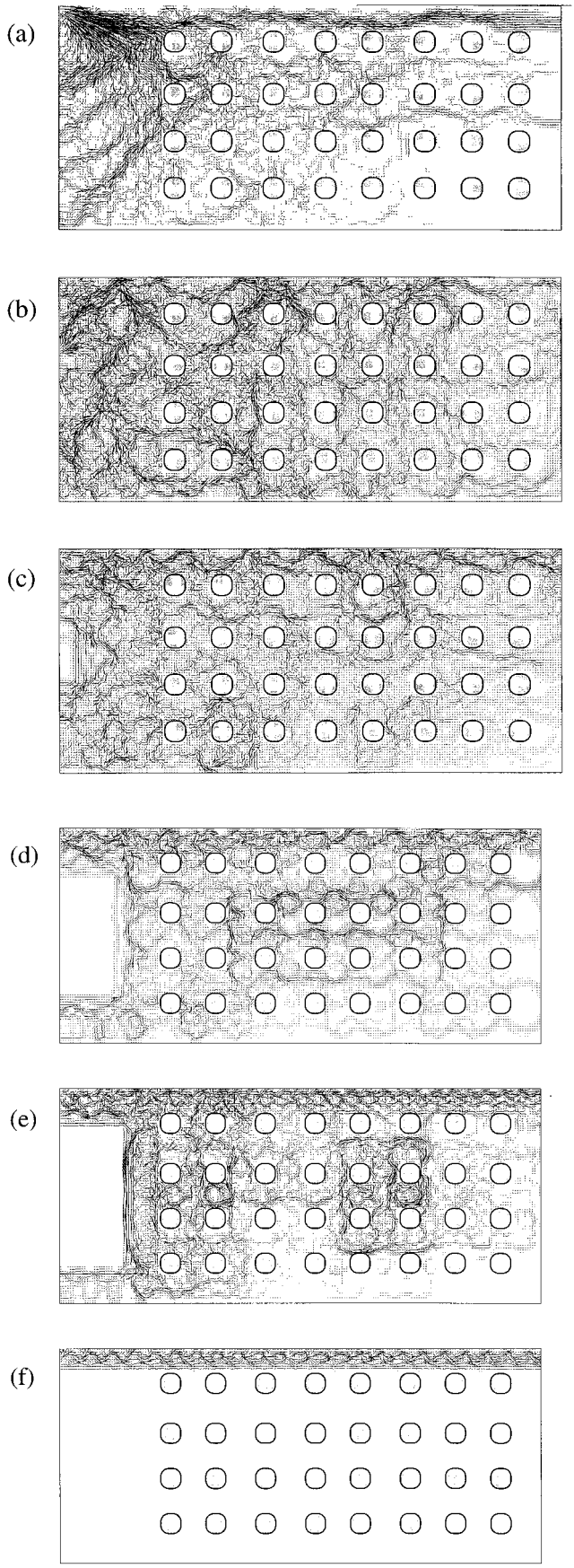

FIG. 3. Current density patterns in the antidot array for different magnetic fields: (a) $B=0$; (b) $B=0.2$ T; (c) $B=0.4$ T ($B\approx B_c/2$); (d) $B=0.7$ T ($B\approx B_c$); (e) $B=0.9$ T; (f) $B=1.5$ T.

the system. In this case electrons travel near the edge without even ''seeing'' the antidot lattice, see Fig. 3(f).

Visualized current density patterns, along with the calculated transmission coefficients, T_{ij}, provide us with valuable information which makes it possible to discuss with confidence the calculated and observed features of the longitudinal magnetoresistance R_L. The behavior of the four-terminal longitudinal resistance R_L is strongly correlated with the two-terminal resistance R_{2t}, see Fig. 2(b). On the other hand, at relatively low magnetic fields, $B\lesssim 0.5$ T, the two-terminal conductance $G_{2t}=1/R_{2t}$ rather faithfully follows the number of Bloch states (NOS) in the infinte antidot lattice (see paper II). Thus, low-field features in the magnetoresistance reflect the band structure of a periodic antidot potential. In particular, R_{2t} is characterized by a broad minimum at $B\sim B_c/2$ (which corresponds to an enhancement of the conductance and increase of the NOS). The transmission coefficient T_{21} is enhanced as well, and the corresponding current density, as discussed above, shows a significant fraction of the electrons traveling between the horizontal rows of antidots. This is consistent with the classical concept of runaway trajectories bouncing off every other antidot in a row, at $B=B_c/2$. It is *inconsistent* with the picture of electrons trapped in orbits around four antidots. Note that when the Landauer-Büttiker formalism is used to express R_L in terms of the transmission coefficients, keeping leading terms only (in this field regime), one arrives at the approximate relation $R_L\approx T_{31}/T_{21}T_{13}$. Since T_{13} is qualitatively similar to T_{21}, we can discuss R_L in terms of

$$R_L\sim T_{31}/T_{21}^2. \tag{1}$$

It follows from Eq. (1) that the enhancement of the transmission coefficient T_{21} near $B=B_c/2$ causes a pronounced minimum of the longitudinal magnetoresistance.

With a further increase of the magnetic field, the number of incoming states in the leads decreases much faster than the NOS in the antidot array. As a result, incoming states in the leads are not able to closely match all the Bloch states in the antidot lattice, and the structure of NOS can hardly be traced any longer in the conductance. In the field region where $B\sim B_c$, R_L shows a broad, but distinct, maximum. We attribute this maximum to the existence of the runaway-type states. Indeed, in the region $B_c/2<B<B_c$, the transmission coefficient T_{21} decreases. At the same time T_{31} is more or less constant, i.e., it is enhanced on the background of an overall decay due to gradually increasing efficiency of edge state transport. This behavior of the transmission coefficients shows that electrons entering the antidot lattice via lead 1 are redirected into lead 3. This occurs via runaway-type states along the leftmost vertical column of the array. The current pattern of Fig. 3(d) demonstrates this. It is worth mentioning that pinned trajectories would cause the opposite effect of a reduction of T_{31} near B_c. With a further increase of the magnetic field beyond B_c runaway states no longer exist. Thus, in this field region, T_{31} rapidly decreases. As a result, electrons entering the lattice from lead 1, predominantly exit from lead 2, with a resulting increase of T_{21}.

The above behavior of the transmission coefficients near B_c (approximate constancy of T_{31}, and a local broad minimum in T_{21}) causes, according to Eq. (1), the broad maximum of the longitudinal resistance, R_L. Note that this maximum, accompanied by an approximate constancy of the (transverse) transmission, T_{31}, is consistent with the similar behavior of the magnetoresistivity in macroscopic rectangular (nonsquare) arrays.[12] In the latter, increase of the diagonal magnetoresistance in one direction (say ρ_{xx}) is related to an increase of the diagonal conductivity in the other direction (σ_{yy}).

When the magnetic field is well above B_c, R_L is greatly reduced due to an increase of efficiency of edge state transport and due to the reduction of the number of bulk Bloch states. The oscillatory structure in R_L observed in this field region, reflects the existence of bulk quasibound states, where electrons are localized between or around antidots [see Fig. 3(e)]. In this field region, transport through the antidot lattice resembles that of the extreme quantum regime considered in Ref. 27.

To conclude this section we stress that our analysis is restricted to the case when the distance between antidots is somewhat larger than the antidot size. This corresponds to the experiment[22] which we try to model. Other experimental studies[11] show that in antidot lattices with large aspect ratios ''antidot size/lattice period,'' quasipinned orbits dominate over runaway trajectories. Classical simulations of the magnetoconductance in antidot arrays with different aspect ratios are discussed in terms of dominating trajectories in Ref. 28.

Our model is an idealized one with a lattice of identical antidots and absence of impurity scattering. Accounting for fluctuations in antidot size and lattice constant, as well as for effects of impurities, one would bring the theory[29] closer to experiment. However, commensurate peaks and quantum oscillations would survive in the magnetoresistence of antidot arrays, if the deviations from an ideal ordering are not too large[12,29] and the scattering from disorder is not too strong.[29]

III. CONCLUSIONS

We have presented a quantum-mechanical study of magnetotransport in a finite antidot lattice in a confined four-terminal geometry. The calculated longitudinal magnetoresistance reproduces the experimental results of Schuster *et al.*,[22] including peak positions of the broad commensurate resonances, as well as the periodicity of the quantum oscillations. By visualizing current density patterns in the antidot array we relate the features in the magnetoresistance to particular types of semiclassical trajectories dominating electron dynamics at a given magnetic field. We find that the current density patterns closely match the character of the corresponding Bloch states in infinite arrays. In our analysis of the commensurate peaks we pinpoint the importance of classical runaway trajectories. In particular, the pronounced peak in the magnetoresistance detected at $B=B_c$, we attribute to relative enhancement of the transmission in the *transverse* direction, caused by the runaway states along the leftmost vertical column of antidots. At the magnetic field of the second commensurate ''resonance,'' $B=B_c/2$, the longitudinal resistance exhibits a pronounced minimum. This we relate to the enhancement of the transmission in the *longitudinal* direction due to the runaway states.

ACKNOWLEDGMENTS

The authors appreciate discussions with T. Ando, K.-F. Berggren, K. Ensslin, S. Ishizaka, R. Schuster, and S. Uryu. I.V.Z. acknowledges support of the Royal Swedish Academy of Sciences and the Norwegian Research Council. He also enjoyed the hospitality of the group of theoretical physics at the Norwegian University of Science and Technology, where this work was started. Finally, F.A.M. acknowledges financial support from the Norwegian Research Council.

[1] K. Ensslin, P. M. Petroff, Phys. Rev. B **41**, 12 307 (1990).
[2] C. G. Smith, M. Pepper, R. Newbury, H. Ahmed, D. G. Hasko, D. C. Peacock, J. E. F. Frost, D. A. Ritchie, G. A. C. Jones, and G. Hill, J. Phys., Condens. Matter **2**, 3405 (1990).
[3] A. Lorke, J. P. Kotthaus, and K. Ploog, Phys. Rev. B **44**, 3447 (1991).
[4] D. Weiss, M. L. Roukes, A. Menschig, P. Grambow, K. von Klitzing, and G. Weimann, Phys. Rev. Lett. **66**, 2790 (1991).
[5] G. M. Gusev, Z. D. Kvon, L. V. Litvin, Yu. V. Nastaushev, A. K. Kalagin, and A. I. Toropov, Pis'ma Zh. Éksp. Teor. Fiz. **55**, 129 (1991) [JETP Lett. **55**, 123 (1992)].
[6] See series of articles in *The Physics of Semiconductors*, edited by M. Scheffler and R. Zimmermann (World Scientific, Singapore, 1996), Vol. 2, pp. 1489–1528.
[7] I. V. Zozoulenko, F. A. Maaø, and E. H. Hauge, Phys. Rev. B **53**, 7975 (1996).
[8] I. V. Zozoulenko, F. A. Maaø, and E. H. Hauge, Phys. Rev. B **53**, 7987 (1996).
[9] R. Fleischmann, T. Geisel, and R. Ketzmerick, Phys. Rev. Lett. **68**, 1367 (1992).
[10] E. M. Baskin, G. M. Gusev, Z. D. Kvon, A. G. Pogosov, and M. V. Entin, Pis'ma Zh. Éksp. Teor. Fiz. **55**, 649 (1992) [JETP Lett. **55**, 678 (1992)].
[11] R. Schuster, G. Ernst, K. Ensslin, M. Entin, M. Holland, G. Böhm, and W. Klein, Phys. Rev. B **50**, 8090 (1994).
[12] K. Tsukagoshi, M. Haraguchi, S. Takaoka, and K. Murase, J. Phys. Soc. Jpn. **65**, 811 (1996).
[13] R. Kaiser, B. Irmer, M. Wendel, T. Schlösser, H. Lorenz, A. Lorke, K. Ensslin, and J. P. Kotthaus, in *The Physics of Semiconductors* (Ref. 6), p. 1501.
[14] D. Weiss, K. Richter, A. Menschig, R. Bergmann, H. Schweizer, K. von Klitzing, and G. Weimann, Phys. Rev. Lett. **70**, 4118 (1993).
[15] F. Nihey, S. W. Hwang, and K. Nakamura, Phys. Rev. **51**, 4649 (1995).
[16] R. B. S. Oakeshott and A. MacKinnon, J. Phys., Condens. Matter **6**, 1519 (1994).
[17] H. Silberbauer and U. Rössler, Phys. Rev. B **50**, 11 911 (1994).
[18] S. Ishizaka, N. Nihey, K. Nakamura, J. Sone, and T. Ando, Phys. Rev. B **51**, 9881 (1995).

[19] S. Uryu and T. Ando, Phys. Rev. B **53**, 13 613 (1996).
[20] T. Nakanishi and T. Ando, Phys. Rev. B **54**, 8021 (1996).
[21] G. Hackenbroich and F. von Oppen, Europhys. Lett. **29**, 151 (1995).
[22] R. Schuster, K. Ensslin, D. Wharam, S. Kühn, J. P. Kotthaus, G. Böhm, W. Klein, G. Tränkle, and G. Weimann, Phys. Rev. B **49**, 8510 (1994).
[23] R. Landauer, IBM J. Res. Dev. **1**, 223 (1957); M. Büttiker, Phys. Rev. Lett. **57**, 1761 (1986).
[24] C. W. J. Beenakker and H. van Houten, in *Solid State Physics: Advances in Research and Applications*, edited by H. Ehrenreich and D. Turnbull (Academic, San Diego, 1991), Vol. 44.; S. Datta, *Electronic Transport in Mesoscopic Systems* (Cambridge University Press, Cambridge, 1995).
[25] R. G. Mani, K. von Klitzing, and K. Ploog, Phys. Rev. B **51**, 2584 (1995).
[26] R. Fleischmann, T. Geisel, R. Ketzmerick, and G. Petschel, Semicond. Sci. Technol. **9**, 1902 (1994).
[27] I. V. Zozulenko, F. A. Maaø, and E. H. Hauge, Phys. Rev. B **51**, 7058 (1995).
[28] S. Ishizaka and T. Ando (unpublished).
[29] S. Uryu and T. Ando, in *The Physics of Semiconductors* (Ref. 6), p. 1505.